Inorganic Chemistry
Article

Inorg. Chem. **2010**, *49*, 10579–10589 **10579**
DOI: 10.1021/ic101594d

Mn_8 and Mn_{16} Clusters from the Use of 2-(Hydroxymethyl)pyridine, and Comparison with the Products from Bulkier Chelates: A New High Nuclearity Single-Molecule Magnet

Taketo Taguchi,[†] Wolfgang Wernsdorfer,[‡] Khalil A. Abboud,[†] and George Christou*[,†]

[†]*Department of Chemistry, University of Florida, Gainesville, Florida 32611-7200, United States, and*
[‡]*Institut Néel, CNRS and Université J. Fourier, BP 166, 38042 Grenoble Cedex 9, France*

Received August 6, 2010

The synthesis, crystal structures, and magnetochemical characterization of two new Mn clusters $[Mn_8O_2(O_2CPh)_{10}(hmp)_4(MeOH)_2]$ (**1**; $6Mn^{II}$, $2Mn^{III}$) and $[Mn_{16}O_8(OH)_2(O_2CPh)_{12}(hmp)_{10}(H_2O)_2](O_2CPh)_2$ (**2**; $6Mn^{II}$, $10Mn^{III}$) are reported. They were obtained from the use of 2-(hydroxymethyl)pyridine (hmpH) under the same reaction conditions but differing in the presence or absence of added base. Thus, the reaction of hmpH with $Mn(O_2CPh)_2$ in CH_2Cl_2/MeOH led to isolation of octanuclear complex **1**, whereas the analogous reaction in the presence of NEt_3 gave hexadecanuclear complex **2**. Complexes **1** and **2** possess either very rare or unprecedented core structures that are related to each other: that of **1** can be described as a linked pair of incomplete $[Mn_4O_3]$ cubanes, while that of **2** consists of a linked pair of complete $[Mn_4O_4]$ cubanes, on either side of which is attached a tetrahedral $[Mn_4(\mu_4\text{-}O)]$ unit. Solid-state direct current (dc) and alternating current (ac) magnetic susceptibility measurements on **1** and **2** establish that they possess $S = 5$ and 8 ground states, respectively. Complex **2** exhibits frequency-dependent out-of-phase (χ_M'') ac susceptibility signals at temperatures below 3 K suggestive of a single-molecule magnet (SMM). Magnetization versus applied dc field sweeps on single crystals of **2**·10MeOH down to 0.04 K exhibited hysteresis, confirming **2** to be a new SMM. Comparison of the structure of **2** (Mn_{16}) with Mn_{12} or Mn_6 clusters previously obtained under the same reaction conditions but with two Me or two Ph groups, respectively, added next to the alkoxide O atom of hmp^- indicate their influence on the nuclearity and structure of the products as being due to the overall bulk of the chelate plus the decreased ability of the O atom to bridge.

Introduction

Polynuclear Mn clusters have been of great interest from a variety of perspectives, including bioinorganic chemistry and materials science. In the former area, it has been found that a pentanuclear Mn_4Ca cluster is an integral component of the photosystem II reaction center of green plants and cyanobacteria,[1] which is responsible for the light-driven oxidation of water to O_2 gas.[2] From a materials point of view, Mn clusters often possess large numbers of unpaired electrons, offering the potential of acting as repeating units in molecule-based magnetic materials and even of functioning as nanoscale magnetic particles themselves.[3] The latter are called single-molecule magnets (SMMs), which are individual molecules that possess a significant barrier (versus kT) to magnetization relaxation and thus exhibit the ability to function as magnets below the blocking temperature (T_B). Many polynuclear clusters containing 3d transition metals have now been discovered to be SMMs,[4−6] the vast majority of which are Mn complexes[7] because Mn clusters often display relatively large ground state S values, as well as negative D values (easy-axis

*To whom correspondence should be addressed. E-mail: christou@chem.ufl.edu. Phone: +1-352-392-8314. Fax: +1-352-392-8757.

(1) (a) Ferreira, K. N.; Iverson, T. M.; Maghlaoui, K.; Barber, J.; Iwata, S. *Science* **2004**, *303*, 1831. (b) Carrell, T. G.; Tyryshkin, A. M.; Dismukes, G. C. *J. Biol. Inorg. Chem.* **2002**, *7*, 2. (c) Cinco, R. M.; Rompel, A.; Visser, H.; Aromi, G.; Christou, G.; Sauer, K.; Klein, M. P.; Yachandra, V. K. *Inorg. Chem.* **1999**, *38*, 5988. (d) Yachandra, V. K.; Sauer, K.; Klein, M. P. *Chem. Rev.* **1996**, *96*, 2927.

(2) (a) Barber, J. *Inorg. Chem.* **2008**, *47*, 1700–1710. (b) Barber, J.; Murray, J. W. *Phil. Trans. R. Soc. B* **2008**, *363*, 1129–1138.

(3) (a) Bagai, R.; Christou, G. *Chem. Soc. Rev.* **2009**, *38*(4), 1011, and references cited therein. (b) Christou, G.; Gatteschi, D.; Hendrickson, D. N.; Sessoli, R. *MRS Bull.* **2000**, *25*, 66.

(4) For example, see: (a) Sessoli, R.; Gatteschi, D.; Caneschi, A.; Novak, M. A. *Nature* **1993**, *365*, 141. (b) Sessoli, R.; Tsai, H. L.; Schake, A. R.; Wang, S. Y.; Vincent, J. B.; Folting, K.; Gatteschi, D.; Christou, G.; Hendrickson, D. N. *J. Am. Chem. Soc.* **1993**, *115*, 1804.

(5) (a) Gatteschi, D.; Sessoli, R.; Cornia, A. *Chem. Commun.* **2000**, 725. (b) Sun, Z. M.; Grant, C. M.; Castro, S. L.; Hendrickson, D. N.; Christou, G. *Chem. Commun.* **1998**, 721. (c) Yang, E. C.; Hendrickson, D. N.; Wernsdorfer, W.; Nakano, M.; Zakharov, L. N.; Sommer, R. D.; Rheingold, A. L.; Ledezma-Gairaud, M.; Christou, G. *J. Appl. Phys.* **2002**, *91*, 7382.

(6) (a) Andres, H.; Basler, R.; Blake, A. J.; Cadiou, C.; Chaboussant, G.; Grant, C. M.; Gudel, H. U.; Murrie, M.; Parsons, S.; Paulsen, C.; Semadini, F.; Villar, V.; Wernsdorfer, W.; Winpenny, R. E. P. *Chem.—Eur. J.* **2002**, *8*, 4867. (b) Murugesu, M.; Mishra, A.; Wernsdorfer, W.; Abboud, K. A.; Christou, G. *Polyhedron* **2006**, *25*, 613.

Published on Web 10/20/2010

Scheme 1

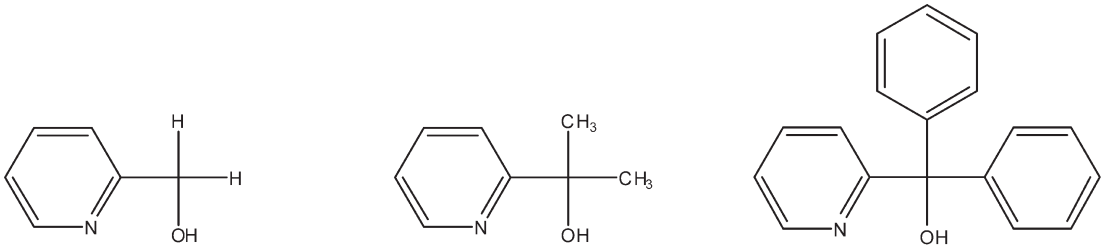

hmpH dmhmpH dphmpH

anisotropy) associated with the presence of Jahn−Teller axially distorted Mn^{III} atoms.

For the above reasons, there is a continuing need for new synthetic routes to metal clusters and SMMs. Our own group has contributed a variety of such methods over the last several years, from "reductive aggregation" of MnO_4^- as a route to new Mn_{12} and Mn_{16} clusters,[8] to a methanolysis procedure to a giant Mn_{84} torus,[9] and a number of others. A generally useful route explored by many groups has been the use of a chelate containing one or more alcohol functionalities, which on deprotonation favor bridging to at least two metal atoms and thus fostering formation of high nuclearity products.[10−16]

One challenge that we recently took on was to see whether for a particular alcohol-containing chelate type we could develop some level of even rudimentary control of the nuclearity of the obtained products by introducing controlled modifications to the chelating/bridging ligand. One favored approach that we have been investigating has involved the introduction of substituents of controllable bulk near the alkoxide functional group of a well explored ligand type to see if and how they might affect the identity of the products compared to those given by the unmodified ligand. Even if the nuclearity was not affected, this seemed at the very least to be a way of potentially perturbing the structures and resulting magnetic properties, but we were optimistic that it would also prove a source of new species with altered nuclearity and interesting structural and magnetic properties. Initial work has concentrated on 2-(hydroxymethyl)pyridine (hmpH), one of the first alcohol-containing chelates employed in Mn cluster chemistry[17] and which has since been found to be the source of many products of various nuclearity.[18−21] We replaced the H atoms at the CH_2 position of the alcohol arm with either Me and Ph groups to give diphenyl-hmpH (dphmpH) and dimethyl-hmpH (dmhmpH) (Scheme 1) and found that the resulting deprotonated groups indeed led to very different products than did hmp^-.[22] In general, it was

(7) (a) Christou, G. *Polyhedron* **2005**, *24*, 2065. (b) Gatteschi, D.; Sessoli, R.; Villain, J.; *Molecular Nanomagnets*; Oxford University Press: New York, 2006. (c) Aromi, G.; Brechin, E. K. *Struct. Bonding* (*Berlin*) **2006**, *122*, 1, and references therein.

(8) (a) King, P.; Wernsdorfer, W.; Abboud, K. A.; Christou, G. *Inorg. Chem.* **2004**, *43*, 7315. (b) Tasiopoulos, A. J.; Wernsdorfer, W.; Abboud, K. A.; Christou, G. *Inorg. Chem.* **2005**, *44*, 6324.

(9) Tasiopoulos, A. J.; Vinslava, A.; Wernsdorfer, W.; Abboud, K. A.; Christou, G. *Angew. Chem., Int. Ed.* **2004**, *43*, 2117.

(10) (a) Foguet-Albiol, D.; O'Brien, T. A.; Wernsdorfer, W.; Moulton, B.; Zaworotko, M. J.; Abboud, K. A.; Christou, G. *Angew. Chem., Int. Ed.* **2005**, *44*, 897. (b) Bagai, R.; Abboud, K. A.; Christou, G. *Inorg. Chem.* **2008**, *47*, 621. (c) Murugesu, M.; Wernsdorfer, W.; Abboud, K. A.; Christou, G. *Angew. Chem., Int. Ed.* **2005**, *44*, 892.

(11) (a) Brechin, E. K. *Chem. Commun.* **2005**, 5141. (b) Milios, C. J.; Vinslava, A.; Wernsdorfer.; Prescimone, A.; Wood, P. A.; Parsons, S.; Perlepes, S. P.; Christou, G.; Brechin, E. K. *J. Am. Chem. Soc.* **2007**, *129*, 6547. (c) Milios, C. J.; Inglis, R.; Vinslava, A.; Bagai, R.; Wernsdorfer, W.; Parsons, S.; Perlepes, S. P.; Christou, G.; Brechin, E. K. *J. Am. Chem. Soc.* **2007**, *129*, 12505.

(12) (a) Moushi, E. E.; Masello, A.; Wernsdorfer, W.; Nastopoulos, V.; Christou, G.; Tasiopoulos, A. J. *Dalton Trans.* **2010**, 4978. (b) Moushi, E. E.; Stamatatos, T. C.; Wernsdorfer, W.; Nastopoulos, V.; Christou, G.; Tasiopoulos, A. J. *Inorg. Chem.* **2009**, *48*, 5049. (c) Tasiopoulos, A. J.; Perlepes, S. P. *Dalton Trans.* **2008**, 5537.

(13) (a) Langley, S. K.; Chilton, N. F.; Massi, M.; Moubaraki, B.; Berry, K. J.; Murray, K. S. *Dalton Trans.* **2010**, 7236. (b) Wittick, L. M.; Jones, L. F.; Jensen, P.; Moubaraki, B.; Spiccia, L.; Berry, K. J.; Murray, K. S. *Dalton Trans.* **2006**, 1534. (c) Wittick, L. M.; Murray, K. S.; Moubaraki, B.; Batten, S. R.; Spiccia, L.; Berry, K. J. *Dalton Trans.* **2004**, 1003.

(14) (a) Milios, C. J.; Kefalloniti, E.; Raptopoulou, C. P.; Terzis, A.; Vicente, R.; Lalioti, N.; Escuer, A.; Perlepes, S. P. *Chem. Commun.* **2003**, 819. (b) Milios, C. J.; Kyritsis, P.; Raptopoulou, C. P.; Terzis, A.; Vicente, R.; Escuer, A.; Perlepes, S. P. *Dalton Trans.* **2005**, 501. (c) Milios, C. J.; Raptopoulou, C. P.; Terzis, A.; Vicente, R.; Escuer, A.; Perlepes, S. P. *Inorg. Chem. Commun.* **2003**, *6*, 1056.

(15) (a) Nayak, S.; Beltran, L. M. C.; Lan, Y.; Clerac, R.; Hearns, N. G. R.; Wernsdorfer, W.; Anson, C. E.; Powell, A. K. *Dalton Trans.* **2009**, 1901. (b) Nayak, S.; Lan, Y.; Clérac, R.; Ansona, C. E.; Powell, A. K. *Chem. Commun.* **2008**, 5698. (c) Ako, A. M.; Hewitt, I. J.; Mereacre, V.; Clérac, R.; Wernsdorfer, W.; Anson, C. E.; Powell, A. K. *Angew. Chem., Int. Ed.* **2006**, *45*, 4926.

(16) (a) Saalfrank, R. W.; Scheurer, A.; Prakash, R.; Heinemann, F. W.; Nakajima, T.; Hampel, F.; Leppin, R.; Pilawa, B.; Rupp, H.; Muller, P. *Inorg. Chem.* **2007**, *46*, 1586. (b) Saalfrank, R. W.; Nakajima, T.; Mooren, N.; Scheurer, A.; Maid, H.; Hampel, F.; Trieflinger, C.; Daub, J. *Eur. J. Inorg. Chem.* **2005**, 1149. (c) Saalfrank, R. W.; Bernt, I.; Chowdhry, M. M.; Hampel, F.; Vaughan, G. B. M. *Chem.—Eur. J.* **2001**, *7*, 2765.

(17) Bouwman, E.; Bolcar, M. A.; Libby, E.; Huffman, J. C.; Folting, K.; Christou, G. *Inorg. Chem.* **1992**, *31*, 5185.

(18) (a) Harden, N. C.; Bolcar, M. A.; Wernsdorfer, W.; A. Abboud, K.; Streib, W. E.; Christou, G. *Inorg. Chem.* **2003**, *42*, 7067. (b) Boskovic, C.; Brechin, E.; Streib, W. E.; Folting, K.; Bollinger, J. C.; Hendrickson, D. N.; Christou, G. *J. Am. Chem. Soc.* **2002**, *124*, 3725. (c) Stamatatos, T. C.; Abboud, K. A.; Wernsdorfer, W.; Christou, G. *Angew. Chem., Int. Ed.* **2006**, *45*, 4134.

(19) (a) Sanudo, E. C.; Brechin, E. K.; Boskovic, C.; Wernsdorfer, W.; Yoo, J.; Yamaguchi, A.; Concolino, T. R.; Abboud, K. A.; Rheingold, A. L.; Ishimoto, H.; Hendrickson, D. N.; Christou, G. *Polyhedron* **2003**, *22*, 2267. (b) Sanudo, E. C.; Wernsdorfer, W.; Abboud, K. A.; Christou, G. *Inorg. Chem.* **2004**, *43*, 4137.

(20) (a) Yoo, J.; Yamaguchi, A.; Nakano, M.; Krzystek, J.; Streib, W. E.; Brunel, L.-C.; Ishimoto, H.; Christou, G.; Hendrickson, D. N. *Inorg. Chem.* **2001**, *40*, 4604. (b) Lecren, L.; Roubeau, O.; Li, Y.-G.; Le Goff, X. F.; Miyasaka, H.; Richard, F.; Wernsdorfer, W.; Coulon, C.; Clérac, R. *Dalton Trans.* **2008**, 755. (c) Miyasaka, H.; Nakata, K.; Lecren, L.; Coulon, C.; Nakazawa, Y.; Fujisaki, T.; Sugiura, K.; Yamashita, M.; Clérac, R. *J. Am. Chem. Soc.* **2006**, *128*, 3770.

(21) (a) Lecren, L.; Wernsdorfer, W.; Li, Y.-G.; Roubeau, O.; Miyasaka, H.; Clerac, R. *J. Am. Chem. Soc.* **2005**, *127*, 11311. (b) Lecren, L.; Li, Y.-G.; Wernsdorfer, W.; Roubeau, O.; Miyasaka, H.; Clerac, R. *Inorg. Chem. Commun.* **2005**, *8*, 626. (c) Lecren, L.; Roubeau, O.; Coulon, C.; Li, Y.-G.; Le Goff, X. F.; Wernsdorfer, W.; Miyasaka, H.; Clerac, R. *J. Am. Chem. Soc.* **2005**, *127*, 17353. (d) Yang, E.-C.; Harden, N.; Wernsdorfer, W.; Zakharov, L. N.; Brechin, E. K.; Rheingold, A. L.; Christou, G.; Hendrickson, D. N. *Polyhedron* **2003**, *22*, 1857.

(22) (a) Taguchi, T.; Daniels, M. R.; Abboud, K. A.; Christou, G. *Inorg. Chem.* **2009**, *48*, 9325. (b) Taguchi, T.; Wernsdorfer, W.; Abboud, K. A.; Christou, G. *Inorg. Chem.* **2010**, *49*, 199.

clear that the two large Ph groups in dphmp$^-$ essentially blocked the ability of the alkoxide O atom to bridge and this group instead favors a bidentate chelating mode. However, in trying to expand these studies and accomplish more detailed comparisons between the products of hmpH, dmhmpH and dphmpH, it was imperative to compare products obtained under exactly the same reaction conditions, and we realized that some important "control" experiments with hmpH were not available for comparison with some dmhmp$^-$ and dphmp$^-$ products we had obtained. We have therefore gone back and further studied the use of hmpH in Mn cluster chemistry.

In the present paper, we report (i) the use of hmpH in reactions with Mn reagents under the same conditions previously employed for dmhmpH and dphmpH reactions; (ii) the structure and magnetic properties of the new Mn_8 and Mn_{16} clusters that have resulted from these hmpH reactions; and (iii) a structural comparison of the clusters from the three ligand types and conclusions about the influence of the added substituents and their increasing bulk on the resulting clusters and their nuclearities. This also provides important lessons for the design of new chelates for further studies in the future.

Experimental Section

Syntheses. All manipulations were performed under aerobic conditions using chemicals and solvents as received, unless otherwise stated.

[$Mn_8O_2(O_2CPh)_{10}(hmp)_4(MeOH)_2$] (1). To a stirred solution of hmpH (0.055 g, 0.50 mmol) in CH_2Cl_2/MeOH (31 mL, 30:1 v/v) was added solid $Mn(O_2CPh)_2$ (0.33 g, 1.0 mmol). The resulting light brown solution was stirred overnight, filtered, and the filtrate carefully layered with hexanes (60 mL). X-ray quality crystals of **1**·CH_2Cl_2 slowly grew over 2 weeks, and they were collected by filtration, washed with CH_2Cl_2/hexanes (2 × 5 mL, 1:1 v/v) and Et_2O (2 × 5 mL), and dried under vacuum; the yield was 61%. Anal. Calcd (Found) for **1**·H_2O ($C_{96}H_{84}N_4Mn_8O_{29}$): C, 52.48 (52.32); H, 3.85 (3.61); N, 2.55 (2.49). Selected IR data (cm^{-1}): 3446(wb), 3064(w), 2928(w), 2836(w), 1967(w), 1919(w), 1601(s), 1560(s), 1489(w), 1397(s), 1294(w), 1174(w), 1154(w), 1069(m), 1042(m), 1027(m), 938(w), 839(w), 759(m), 718(s), 689(m), 675(m), 637(m), 622(m), 603(m), 575(m), 508(w), 415(m).

[$Mn_{16}O_8(OH)_2(O_2CPh)_{12}(hmp)_{10}(H_2O)_2$]($O_2CPh)_2$ (2). To a stirred solution of hmpH (0.11 g, 1.0 mmol) and NEt_3 (0.42 mL, 3.0 mmol) in CH_2Cl_2/MeOH (31 mL, 30:1 v/v) was added solid $Mn(O_2CPh)_2$ (0.33 g, 1.0 mmol). The resulting dark brown solution was stirred overnight, filtered, and the filtrate carefully layered with hexanes (60 mL). X-ray quality crystals of **2**·10MeOH formed over 3 weeks, and they were collected by filtration, washed with CH_2Cl_2/hexanes (2 × 5 mL, 1:1 v/v) and Et_2O (2 × 5 mL), and dried under vacuum; the yield was 30%. Anal. Calcd (Found) for **2**·H_2O ($C_{158}H_{138}N_{10}Mn_{16}O_{51}$): C, 49.01 (49.00); H, 3.59 (3.61); N, 3.62 (3.46). Selected IR data (cm^{-1}): 3446(wb), 3060(w), 2904(w), 2813(w), 1604(s), 1564(s), 1486(w), 1395(s), 1289(w), 1218(w), 1175(w), 1154(w), 1078(m), 1049(m), 1025(m), 833(w), 757(m), 719(s), 677(m), 635(m), 603(m), 544(w), 509(w), 463(w), 430(w), 410(w).

X-ray Crystallography. For **1**·CH_2Cl_2, data were collected on a Siemens SMART PLATFORM equipped with a CCD area detector and a graphite monochromator utilizing Mo K_α radiation (λ = 0.71073 Å). Suitable crystals were attached to glass fibers using silicone grease and transferred to a goniostat where they were cooled to 100 K for data collection. Cell parameters were refined using 8192 reflections. A full sphere of data (1850 frames) was collected using the ω-scan method (0.3° frame width). The first 50 frames were remeasured at the end of data collection to monitor instrument and crystal stability (maximum correction on I was < 1%). Absorption corrections by integration were applied based on measured indexed crystal faces. For **2**·10MeOH, data were collected at 100 K on a Bruker DUO system equipped with an APEX II area detector and a graphite monochromator utilizing Mo K_α radiation. Cell parameters were refined using 9999 reflections. A hemisphere of data was collected using the ω-scan method (0.5° frame width). Absorption corrections by integration were applied based on measured indexed crystal faces. The structures were solved by direct methods in SHELXTL6,[23] and refined on F^2 using full-matrix least-squares. The non-H atoms were refined anisotropically, whereas the H atoms were placed in calculated, ideal positions and refined as riding on their respective C atoms.

Table 1. Crystallographic Data for **1**·CH_2Cl_2 and **2**·10MeOH

	1	**2**
formula[a]	$C_{97}H_{84}Cl_2Mn_8N_4O_{28}$	$C_{168}H_{176}Mn_{16}N_{10}O_{60}$
fw, g mol^{-1}[a]	2264.10	4174.24
crystal system	triclinic	triclinic
space group	$P\bar{1}$	$P\bar{1}$
a, Å	12.1580(18)	16.821(2)
b, Å	14.407(2)	17.187(2)
c, Å	28.249(4)	27.034(4)
α, deg	103.557(2)	71.970(2)
β, deg	93.985(2)	69.929(2)
γ, deg	94.483(2)	68.573(2)
V, Å^3	4775.8(12)	4618.4(11)
Z	2	1
T, K	100(2)	100(2)
radiation, Å[b]	0.71073	0.71073
ρ_{calc}, g cm^{-3}	1.574	1.386
μ, mm^{-1}	1.159	1.127
$R1$[c,d]	0.0856	0.0715
wR[e,f]	0.1745	0.1760

[a] Including solvate molecules. [b] Graphite monochromator. [c] $I > 2\sigma(I)$. [d] $R1 = \sum||F_o| - |F_c||/\sum|F_o|$. [e] All data. [f] $wR2 = [\sum w(F_o^2 - F_c^2)^2/\sum w(F_o^2)^2]^{1/2}$, $w = 1/[\sigma^2(F_o^2) + [(ap)^2 + bp]$, where a = 0.0220 (**1**) or 0.0844 (**2**), b = 65.7247 (**1**) or 0 (**2**), and $p = [\max(F_o^2, 0) + 2F_c^2]/3$.

For **1**·CH_2Cl_2, the asymmetric unit consists of two half Mn_8 clusters each located on an inversion center, and an ordered CH_2Cl_2 solvate molecule. A total of 1246 parameters were refined in the final cycle of refinement to yield R_1 (10259 reflections with $I > 2\sigma(I)$) and wR_2 (all 16560 reflections) of 8.56 and 17.45%, respectively. For **2**·10MeOH, the asymmetric unit consists of a half Mn_{16} cluster dication located on an inversion center, two half $PhCO_2^-$ counterions, and five MeOH solvate molecules. The latter were too disordered to be modeled properly, and thus program SQUEEZE, a part of the PLATON package of crystallographic software, was used to calculate the solvent disorder area and remove its contribution to the overall intensity data. The counterions were treated as rigid groups and constrained to maintain a geometry as close as possible to ideal. The water (O23) and hydroxyl (O21) protons were obtained from a difference Fourier map; the water protons were treated as riding on the parent O atom while the hydroxyl proton was refined without any constraints. A total of 993 parameters were refined in the final cycle of refinement to yield R_1 (9205 reflections with $I > 2\sigma(I)$) and wR_2 (all 16353 reflections) of 7.15 and 17.60%, respectively. Unit cell data and details of the structure refinements for the two complexes are listed in Table 1.

Other Studies. Infrared spectra were recorded in the solid state (KBr pellets) on a Nicolet Nexus 670 FTIR spectrometer in the 400−4000 cm^{-1} range. Elemental analyses (C, H, and N) were performed by the in-house facilities of the University of Florida, Chemistry Department. Variable-temperature direct current (dc) and alternating current (ac) magnetic susceptibility data were collected using a Quantum Design MPMS-XL SQUID magnetometer equipped with a 7 T magnet and operating in the

(23) *SHELXTL6*; Bruker-AXS: Madison, WI, 2000.

Scheme 2

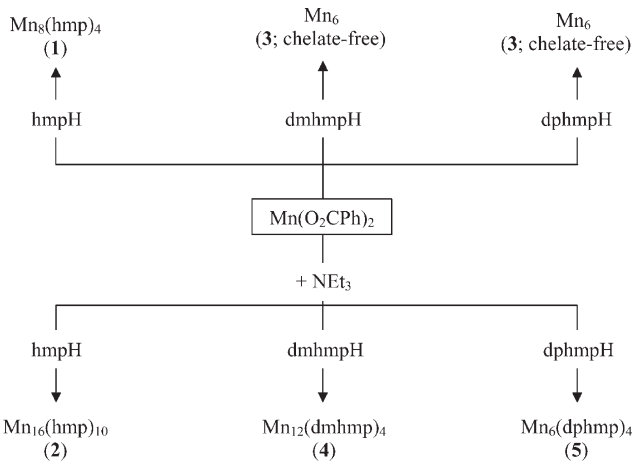

1.8−300 K range. Samples were embedded in solid eicosane to prevent torquing. Pascal's constants[24] were used to estimate the diamagnetic correction, which was subtracted from the experimental susceptibility to give the molar paramagnetic susceptibility (χ_M). Low-temperature (< 1.8 K) hysteresis and dc magnetization relaxation studies were performed at Grenoble using an array of micro-SQUIDS.[25] The high sensitivity of this magnetometer allows the study of single crystals of SMMs of the order of 10−500 μm. The field was applied parallel to the easy axis of the molecule. Crystals were maintained in mother liquor to avoid degradation and were covered with grease for protection during transfer to the micro-SQUID and subsequent cooling.

Results and Discussion

Syntheses. A variety of reaction conditions were systematically explored in arriving at the optimized procedures described below. The reaction of $Mn(O_2CPh)_2$ with hmpH in a 2:1 ratio in CH_2Cl_2/MeOH (30:1) afforded a light brown solution from which was subsequently isolated $[Mn_8O_2(O_2CPh)_{10}(hmp)_4(MeOH)_2]$ (**1**). Its formation is summarized in eq 1, assuming atmospheric O_2 is the oxidizing agent. The mixed solvent system was needed to ensure adequate solubility of all reagents. Small variations

$$8Mn(O_2CPh)_2 + 4hmpH + \frac{1}{2}O_2 + H_2O + 2MeOH \rightarrow [Mn_8O_2(O_2CPh)_{10}(hmp)_4(MeOH)_2] + 6PhCO_2H \quad (1)$$

in the Mn^{II}/hmpH ratio also gave complex **1**. When the same reaction was carried out with either dmhmpH or dphmpH, the isolated product in both cases was the chelate-free complex $[Mn_6O_2(O_2CPh)_{10}(MeOH)_2(H_2O)_2]$ (**3**) with a known and common Mn_6 topology[26,27] (Scheme 2).

In previous studies with dmhmpH and dphmpH, we had found that their reaction with $Mn(O_2CPh)_2$ and NEt_3 in 1:1:3 ratio in CH_2Cl_2/MeOH (30:1 v/v) gave $[Mn_{12}O_7(OH)(OMe)_2(O_2CPh)_{12}(dmhmp)_4(H_2O)]$ (**4**) and $[Mn_6O_4(OMe)_2(O_2CPh)_4(dphmp)_4]$ (**5**), respectively (Scheme 2).[22] In fact, we had never explored hmpH in this exact reaction system, and we now did so to allow a better comparison of the products of the three chelates under identical conditions (vide infra). The reaction was found to give a dark brown solution from which was subsequently obtained the new complex $[Mn_{16}O_8(OH)_2(O_2CPh)_{12}(hmp)_{10}(H_2O)_2](O_2CPh)_2$ (**2**) in 30% yield. Its formation is summarized in eq 2. Small variations in the Mn/hmpH/NEt_3 ratio also gave **2**, but if the NEt_3 was omitted complex **1** was obtained (but in a lower yield of ∼40% than the optimized procedure discussed above). Increasing the amount of MeOH still gave complex **2**, but it was contaminated with a small amount of **1**, suggesting the latter might be an intermediate to the former.

$$16Mn(O_2CPh)_2 + 10hmpH + \frac{5}{2}O_2 + 7H_2O \rightarrow [Mn_{16}O_8(OH)_2(O_2CPh)_{12}(hmp)_{10}(H_2O)_2](O_2CPh)_2 + 18PhCO_2H \quad (2)$$

Although it is clear that the reactions that lead to **1** and **2** are very complicated and both clearly involve acid/base (e.g., water deprotonation to O^{2-}/OH^-) and redox (Mn^{II} oxidation) chemistry, and structural aggregation, it is of interest to note that the only difference in their reaction conditions is the presence or absence of NEt_3, giving **2** and **1**, respectively. In fact, the observations above are consistent with the first product of the reaction being **1** ($6Mn^{II}$, $2Mn^{III}$), whose oxidation level (average $Mn^{2.25+}$) is close to the Mn^{II} starting material and with a correspondingly low O^{2-}/Mn ratio of 1:4. In the presence of NEt_3, which facilitates further oxidation by O_2 and deprotonation of water to generate more OH^-/O^{2-}, **1** undergoes further reaction and the product is **2** ($6Mn^{II}$, $10Mn^{III}$), with a higher oxidation level (average $Mn^{2.63+}$) and a correspondingly higher OH^-/O^{2-}/Mn ratio of 5:8. This interpretation of the reaction also suggests that there might be some structural similarity between **1** and **2**, and this is indeed the case.

Description of Structures. The partially labeled structure, a stereoview, and the labeled core of complex **1** are shown in Figure 1. Selected interatomic distances and angles are listed in Table 2. Complex **1**·CH_2Cl_2 crystallizes in the triclinic space group $P\bar{1}$ with two essentially superimposable independent molecules in the unit cell, both lying on inversion centers; only one will therefore be referred to below. The $[Mn_8(\mu_4\text{-}O)_2(\mu_3\text{-}OR)_4(\mu\text{-}OR)_4]^{6+}$ core can be described as consisting of a central $[Mn_6O_2]^{10+}$ unit (Mn1, Mn2, Mn4 and their symmetry partners) with the commonly observed edge-sharing Mn_6 bitetrahedral structure.[26,27] On each end of this is attached a Mn atom by two μ_3-hmp^- and one benzoate group. The resulting core can also be described as two incomplete cubanes (Mn1, Mn2′, Mn3, Mn4 and Mn1′, Mn2, Mn3′ and Mn4′) joined together by Mn2−O12′ and Mn2′-O12 linkages, with benzoate atoms O3 and O3′ providing additional monatomic bridges. The peripheral ligation is provided by ten benzoate and four hmp^- groups. Charge considerations, the metric parameters,

(24) Weast, R. C. *CRC handbook of Chemistry and Physics*; CRC Press, Inc.: Boca Raton, FL1984.
(25) (a) Wernsdorfer, W. *Adv. Chem. Phys.* **2001**, *118*, 99. (b) Wernsdorfer, W. *Supercond. Sci. Technol.* **2009**, *22*, 064013.
(26) Blackman, A. G.; Huffman, J. C.; Lobkovsky, E. B.; Christou, G. *Polyhedron* **1992**, *11*, 251.
(27) Schake, A. R.; Vincent, J. B.; Li, Q.; Boyd, P. D. W.; Folting, K.; Huffman, J. C.; Hendrickson, D. N.; Christou, G. *Inorg. Chem.* **1989**, *28*, 1915.

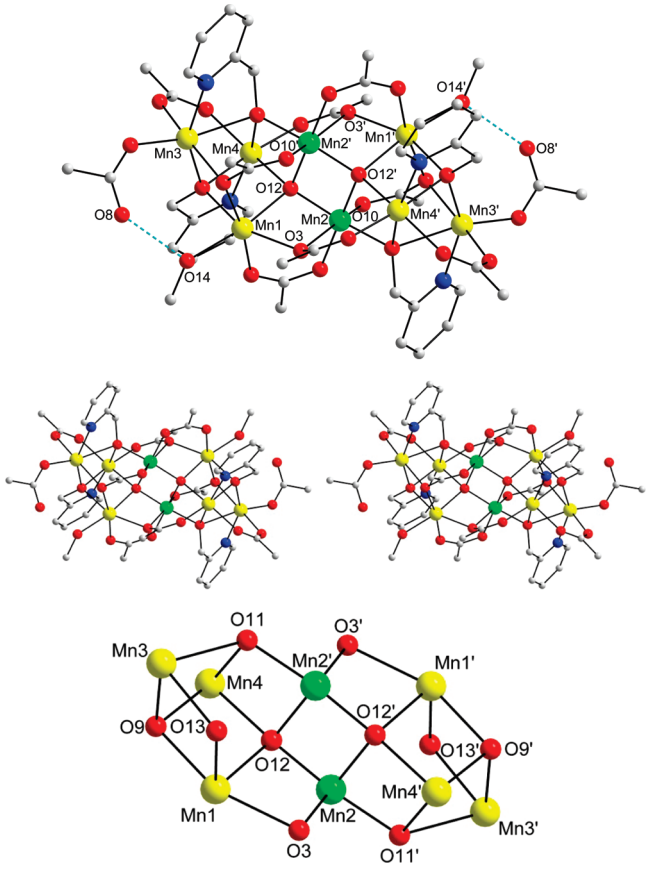

Figure 1. Structure of complex **1** with intramolecular hydrogen-bonds shown as dashed lines (top), a stereopair (middle), and the labeled core. H atoms and Ph rings (except for the *ipso* C atoms) on benzoate groups have been omitted for clarity. Color code: Mn^{II} yellow; Mn^{III} green; O red; N blue; C gray.

Table 2. Selected Interatomic Distances (Å) and Angles (deg) for **1**·CH_2Cl_2

Mn1−O1	2.128(6)	Mn4−O5	2.144(6)
Mn1−O3	2.248(6)	Mn4−O9′	2.214(6)
Mn1−O9	2.189(6)	Mn4−O11′	2.250(6)
Mn1−O12	2.196(6)	Mn4−O12′	2.197(6)
Mn1−O13	2.167(6)	Mn4−N1′	2.190(8)
Mn1−O14	2.163(6)	Mn1−O3−Mn2	87.0(2)
Mn2−O2	1.954(6)	Mn3−O9−Mn1	102.0(2)
Mn2−O3	2.435(6)	Mn3−O9−Mn4′	96.7(2)
Mn2−O10	2.243(6)	Mn1−O9−Mn4′	99.6(2)
Mn2−O11′	1.957(6)	Mn2′−O11−Mn4′	93.9(2)
Mn2−O12	1.882(6)	Mn2′−O11−Mn3	124.4(3)
Mn2−O12′	1.887(6)	Mn4′−O11−Mn3	88.1(2)
Mn3−O6′	2.170(6)	Mn2−O12−Mn2′	96.7(3)
Mn3−O7	2.079(6)	Mn2−O12−Mn1	104.2(3)
Mn3−O9	2.150(6)	Mn2′−O12−Mn1	115.5(3)
Mn3−O11	2.436(6)	Mn2−O12−Mn4′	143.0(3)
Mn3−O13	2.247(6)	Mn2′−O12−Mn4′	97.6(2)
Mn3−N2	2.260(8)	Mn1−O12−Mn4′	99.9(2)
Mn4−O4	2.093(6)	Mn1−O13−Mn3	99.6(2)

and the presence of Mn^{III} Jahn−Teller (JT) distortions (axial elongations) indicate a $Mn^{II}_6Mn^{III}_2$ description with Mn2 and Mn2′ being Mn^{III}, as confirmed by bond valence sum (BVS) calculations (Table 3).[28] As expected, the JT axes on Mn2 and Mn2′ avoid the Mn−O^{2-} bonds and lie on the O3−Mn2−O10 and O3′−Mn2′−O10′ axes. The benzoates display three binding modes: six are in the common $\eta^1{:}\eta^1{:}\mu$ bridging mode, two are in the less common $\eta^2{:}\eta^1{:}\mu_3$ bridging mode, and the remaining two are terminally bound to Mn^{II} atoms Mn3 and Mn3′, with the unbound O atom (O8, O8′) forming a H bond to the adjacent terminal MeOH (O8···O14 = 2.649(11) Å).

(28) (a) Brown, I. D.; Altermatt, D. *Acta Crystallogr.* **1985**, *B41*, 244. (b) Liu, W.; Thorp, H. H. *Inorg. Chem.* **1993**, *32*, 4102.

Table 3. Bond Valence Sums for the Mn Atoms in Complex **1**[a]

atom	Mn^{II}	Mn^{III}	Mn^{IV}
Mn1	1.95	1.79	1.88
Mn2	3.08	2.82	2.96
Mn3	1.88	1.74	1.80
Mn4	2.05	1.90	1.96

[a] The underlined value is the one closest to the charge for which it was calculated, and the nearest whole number can be taken as the oxidation state of that atom.

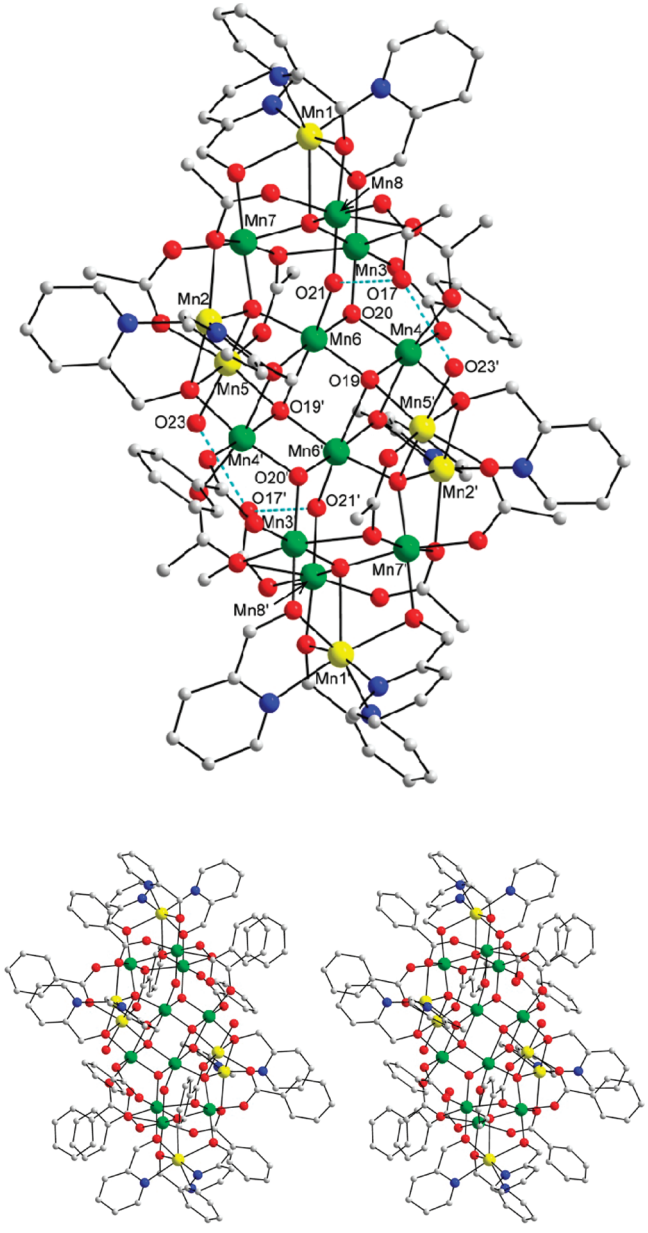

Figure 2. Structure of the cation of **2** with intramolecular hydrogen-bonds shown as dashed lines (top) and a stereopair (bottom). H atoms and Ph rings (except for the *ipso* C atoms) on benzoate groups have been omitted for clarity. Color code: Mn^{II} yellow; Mn^{III} green; O red; C gray; N blue.

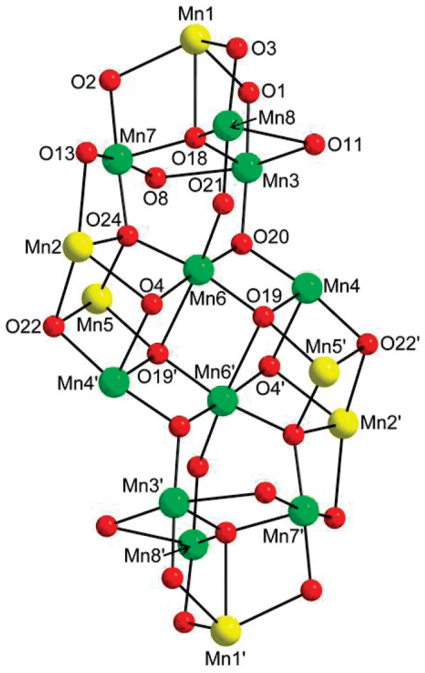

Figure 3. Fully labeled core of complex **2**. Color code: Mn^{II} yellow; Mn^{III} green; O red.

The four hmp^- groups all bind in a $\eta^1{:}\eta^3{:}\mu_3$ mode. All the Mn atoms are six-coordinate with distorted octahedral geometry. While a number of other Mn_8 complexes with a variety of metal topologies such as rodlike, serpentine, rectangular, linked Mn_4 butterfly units, linked tetrahedral, and so forth have been are previously reported,[29−32] the linked incomplete-dicubane core of **1** is very rare, having been seen only once before in Mn chemistry.[33]

The structure and a stereoview of the $[Mn_{16}O_8(OH)_2(hmp)_{10}(O_2CPh)_{12}(H_2O)]^{2+}$ cation of **2** are shown in Figure 2, and its core in Figure 3. Selected interatomic distances and angles are listed in Table 4. The centrosymmetric complex is mixed-valent $Mn^{II}_6Mn^{III}_{10}$, as indicated by the metric parameters and confirmed by BVS calculations (Table 5), and contains an $[Mn_{16}(\mu_4\text{-}O)_6(\mu_3\text{-}O)_2(\mu_3\text{-}OR)_4(\mu\text{-}O)_2(\mu_3\text{-}OR)_{12}]$ core consisting of two now-complete $[Mn_4(\mu_4\text{-}O)_2(\mu_3\text{-}OR)_2]$ cubanes edge-linked together at the Mn6−O19′ and Mn6′-O19 edges, with $\mu_3\text{-}O^{2-}$ ions (O20 and O20′) providing additional monatomic bridges. On each side of this central complete-dicubane is attached a tetrahedral $[Mn_4(\mu_4\text{-}O^{2-})]$ unit (Mn1, Mn3, Mn7, Mn8). The degree of protonation of the inorganic O atoms was established by O BVS calculations (Table 6), revealing six $\mu_4\text{-}O^{2-}$ (O18, O19, O24), two $\mu_3\text{-}O^{2-}$ (O20), two μ-OH (O21), and two terminal H_2O molecules (O23). There are sixteen benzoate groups: ten are in the common $\eta^1{:}\eta^1{:}\mu$ mode, four in the rarer $\eta^2{:}\eta^1{:}\mu_3$ mode, and two are terminally bound to Mn8, with the unbound O atom (O17) forming H-bonds to the nearby μ−OH^- (O17···O21 = 2.652(8) Å) and terminal water (O17···O23′=2.891(12) Å). Among the ten hmp^- groups,

Table 4. Selected Interatomic Distances (Å) and Angles (deg) for **2**·10MeOH

Mn1−O1	2.165(4)	Mn7−O18	1.917(4)
Mn1−O2	2.200(4)	Mn7−O24	1.871(4)
Mn1−O3	2.168(5)	Mn8−O3	1.897(4)
Mn1−N1	2.354(5)	Mn8−O11	2.657(6)
Mn1−N2	2.270(6)	Mn8−O12	2.174(5)
Mn1−N3	2.259(7)	Mn8−O16	1.942(4)
Mn2−O4	2.189(4)	Mn8−O18	1.903(4)
Mn2−O13	2.209(4)	Mn8−O21	1.853(4)
Mn1−O18	2.413(4)	Mn3−O1−Mn1	107.39(19)
Mn2−O22	2.268(4)	Mn7−O2−Mn1	108.92(19)
Mn2−O24	2.140(4)	Mn8−O3−Mn1	107.45(19)
Mn2−N4	2.212(6)	Mn6−O4−Mn2	95.19(17)
Mn2−N5	2.183(6)	Mn6−O4−Mn4′	100.92(17)
Mn3−O1	1.888(4)	Mn2−O4−Mn4′	97.08(15)
Mn3−O6	1.954(4)	Mn7−O8−Mn3	86.46(15)
Mn3−O8	2.379(4)	Mn2−O13−Mn7	90.58(17)
Mn3−O11	2.148(4)	Mn8−O18−Mn7	127.4(2)
Mn3−O18	1.928(4)	Mn8−O18−Mn3	115.5(2)
Mn3−O20	1.874(4)	Mn7−O18−Mn3	110.16(19)
Mn4−O4′	2.290(4)	Mn8−O18−Mn1	98.28(16)
Mn4−O7	1.973(4)	Mn7−O18−Mn1	100.56(17)
Mn4−O10	2.160(4)	Mn3−O18−Mn1	97.14(17)
Mn4−O19	1.882(4)	Mn4−O19−Mn6	96.26(18)
Mn4−O20	1.869(4)	Mn4−O19−Mn5′	101.57(18)
Mn4−O22′	1.949(4)	Mn6−O19−Mn5′	160.9(2)
Mn5−O9	2.124(4)	Mn4−O19−Mn6′	99.06(16)
Mn5−O15	2.122(5)	Mn6−O19−Mn6′	95.15(15)
Mn5−O19′	2.135(4)	Mn5′−O19-Mn6′	88.68(14)
Mn5−O22	2.341(4)	Mn4−O20−Mn3	121.88(19)
Mn5−O23	2.149(4)	Mn4−O20−Mn6	96.20(17)
Mn5−O24	2.158(4)	Mn3−O20−Mn6	125.5(2)
Mn6−O4	1.972(4)	Mn8−O21−Mn6	127.8(3)
Mn6−O19	1.886(4)	Mn4′−O22-Mn2	105.28(18)
Mn6−O19′	2.423(4)	Mn4′−O22-Mn5	92.71(17)
Mn6−O20	1.900(4)	Mn2−O22−Mn5	96.93(15)
Mn6−O21	2.108(4)	Mn7−O24−Mn6	125.95(19)
Mn6−O24	1.930(4)	Mn7−O24−Mn2	106.44(19)
Mn7−O2	1.906(4)	Mn6−O24−Mn2	98.07(17)
Mn7−O8	2.221(4)	Mn7−O24−Mn5	114.7(2)
Mn7−O13	2.316(5)	Mn6−O24−Mn5	102.51(18)
Mn7−O14	1.965(4)	Mn2−O24−Mn5	106.79(16)

Table 5. Bond Valence Sums for the Mn Atoms in Complex **2**[a]

atom	Mn^{II}	Mn^{III}	Mn^{IV}
Mn1	2.06	1.94	1.95
Mn2	2.02	1.89	1.91
Mn3	3.26	2.98	3.13
Mn4	3.25	2.97	3.12
Mn5	2.04	1.86	1.96
Mn6	3.19	2.92	3.06
Mn7	3.20	2.93	3.07
Mn8	3.34	3.05	3.20

[a] See the footnote of Table 3.

(29) (a) Godbole, M. D.; Roubeau, O.; Clerac, R.; Kooijman, H.; Spek, A. L.; Bouwman, E. *Chem. Commun.* **2005**, 3715. (b) Brechin, E. K.; Soler, M.; Christou, G.; Helliwell, M.; Teat, S. J.; Wernsdorfer, W. *Chem. Commun.* **2003**, 1276. (c) Brechin, E. K.; Christou, G.; Soler, M.; Helliwell, M.; Teat, S. J. *Dalton Trans.* **2003**, 513.

(30) (a) Jones, L. F.; Brechin, E. K.; Collison, D.; Raftery, J.; Teat, S. J. *Inorg. Chem.* **2003**, *42*, 6971. (b) Alvareza, C. S.; Bond, A. D.; Cave, D.; Mosquera, M. E. G.; Harron, E. A.; Layfield, R. A.; McPartlin, M.; Rawson, J. M.; Wood, P. T.; Wright, D. S. *Chem. Commun.* **2002**, 2980. (c) Boskovic, C.; Huffman, J. C.; Christou, G. *Chem. Commun.* **2002**, 2502.

(31) (a) Tsai, H. L.; Wang, S. Y.; Folting, K.; Streib, W. E.; Hendrickson, D. N.; Christou, G. *J. Am. Chem. Soc.* **1995**, *117*, 2503. (b) Tanase, S.; Aromi, G.; Bouwman, E.; Kooijman, H.; Spek, A. L.; Reedijk, J. *Chem. Commun.* **2005**, 3147. (c) Milios, C. J.; Kefalloniti, E.; Raptopoulou, C. P.; Terzis, A.; Vicente, R.; Lalioti, N.; Escuer, A.; Perlepes, S. P. *Chem. Commun.* **2003**, 819.

(32) (a) Wemple, M. W.; Tsai, H. L.; Wang, S. Y.; Claude, J. P.; Streib, W. E.; Huffman, J. C.; Hendrickson, D. N.; Christou, G. *Inorg. Chem.* **1996**, *35*, 6437. (b) Tasiopoulos, A. J.; Abboud, K. A.; Christou, G. *Chem. Commun.* **2003**, 580. (c) Milios, C. J.; Fabbiani, F. P. A.; Parsons, S.; Murugesu, M.; Christou, G.; Brechin, E. K. *Dalton Trans.* **2006**, 351. (d) Saalfrank, R. W.; Low, N.; Trummer, S.; Sheldrick, G. M.; Teichert, M.; Stalke, D. *Eur. J. Inorg. Chem.* **1998**, 559.

(33) Boskovic, C.; Wernsdorfer, W.; Folting, K.; Huffman, J. C.; Hendrickson, D. N.; Christou, G. *Inorg. Chem.* **2002**, *41*, 5107.

Table 6. BVS for Selected O Atoms in **2**[a]

atom	BVS	assgt[a]
O18	1.90	O^{2-}
O19	1.76	O^{2-}
O20	1.91	O^{2-}
O21	1.03	OH^{-}
O23	0.33	H_2O
O24	1.87	O^{2-}

[a] The O atom is an O^{2-} if the BVS is ~1.8−2.0, an OH^{-} if it is ~1.0−1.2, and an H_2O if it is ~0.2−0.4, although the ranges can be affected slightly by H-bonding.

four are bridging within the central dicubane in a $\eta^1{:}\eta^3{:}\mu_3$ mode, and the other six are bridging within the outer tetrahedral units in a $\eta^1{:}\eta^2{:}\mu$ mode. The Mn atoms are all six-coordinate with distorted octahedral geometry, except for Mn^{II} atom Mn1, which is seven-coordinate. There are several Mn_{16} clusters known in the literature with wheel-shaped, planar, grid, and so forth structures,[10c,34,35] but none of them possess the metal topology of **2**, which is thus unprecedented.

Interestingly, the structure of complex **2** is similar to that of a previously reported Mn_{12}-benzoate complex with hmp^{-}, $[Mn_{12}O_8Cl_4(O_2CPh)_8(hmp)_6]$ (**6**)[18b] in that both consist of two tetrahedral $[Mn^{II}Mn^{III}_3]$ units bridged by oxide ions to the central unit. The difference is that the central unit of **6** is a face-sharing defective dicubane (Mn^{III}_4) whereas that of **2** is a linked complete-dicubane ($2 \times Mn^{II}_2Mn^{III}_2$); in fact, note that the latter is the former with two additional Mn^{II} atoms at each end.

As stated above, the cores of **1** and **2** thus show some structural relationship in that they both contain a linked dicubane unit; in **1**, each cubane is Mn^{II}_3, Mn^{III} and is incomplete in that one vertex does not contain a triply bridging monatomic bridge, whereas in **2** each cubane is Mn^{II}_2, Mn^{III}_2 and as a result is now complete in this regard. With respect to the suggestion that **1** might be an intermediate to **2**, it is reasonable that further oxidation of **1** and the incorporation of additional bridging OH^{-}/O^{2-} ions would lead to enlargement to a higher nuclearity product. However, the complexity of these reactions and the absence of a discriminating spectroscopic probe make it very difficult to probe this matter further.

Magnetochemistry. Magnetic Susceptibility Study of Complex 1. Variable temperature dc magnetic susceptibility measurements were performed on a microcrystalline powder sample of $\mathbf{1}\cdot H_2O$ in a 0.1 T field and in the 5.0−300 K range. The sample was restrained in eicosane to prevent torquing. The obtained data are shown as a $\chi_M T$ versus T plot in Figure 4. $\chi_M T$ gradually decreases from 25.09 cm^3 K mol^{-1} at 300 K to 15.11 cm^3 K mol^{-1} at 5.0 K. The 300 K value is much less than the spin-only ($g = 2$) value of 29.25 cm^3 K mol^{-1} for six Mn^{II} and two Mn^{III} non-interacting atoms, indicating dominant antiferromagnetic exchange interactions. The plot does not

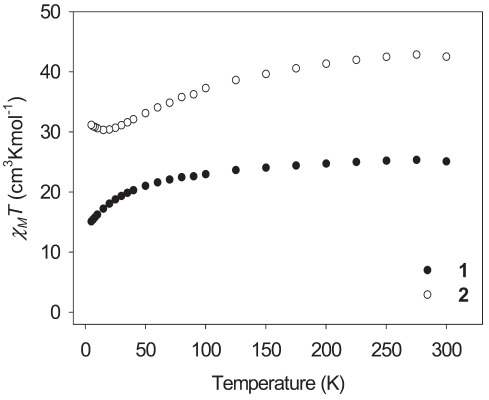

Figure 4. Plots of $\chi_M T$ versus T for complexes **1** and **2**.

appear to be heading to zero at 0 K, indicating that $\mathbf{1}\cdot H_2O$ has an $S > 0$ ground state, and the 5 K value can be compared with the spin-only ($g = 2$) value of 15.00 cm^3 K mol^{-1} for an $S = 5$ state. To determine the ground state of $\mathbf{1}\cdot H_2O$, as well as the magnitude and sign of D, magnetization (M) data were collected in the 1−7 T magnetic field (H) and 1.8−10.0 K temperature ranges. We attempted to fit the data, using the program MAGNET,[36] by diagonalization of the spin Hamiltonian matrix assuming only the ground state is populated, incorporating axial anisotropy ($D\hat{S}_z^2$) and Zeeman terms, and employing a full powder average. The corresponding spin Hamiltonian is given by eq 3, where $\hat{S}_z$ is the easy-axis spin operator, g is the Landé g factor, μ_B is the

$$\mathscr{H} = D\hat{S}_z^{\,2} + g\mu_B\mu_0\hat{S}\cdot H \qquad (3)$$

Bohr magneton, and μ_0 is the vacuum permeability. However, we could not get an acceptable fit using data collected over the whole field range, which is a common problem caused by low-lying excited states, especially if some have an S value greater than that of the ground state, as would be expected for so many weakly coupled Mn^{II} atoms. This conclusion is supported by the M versus H plot (Supporting Information, Figure S1), which does not show saturation but instead a steadily increasing magnetization with H. A common solution is to use only data collected at low fields (≤1.0 T), as we showed for many mixed-valence Mn^{II}/Mn^{III} clusters,[37] but for $\mathbf{1}\cdot H_2O$ it was still not possible to obtain a satisfactory fit, suggesting particularly low-lying excited states. Thus, we turned to ac susceptibility measurements, which are a powerful complement to dc studies for determining the ground state S of a system, because they preclude complications from an applied dc field.[19b,38]

The ac studies on $\mathbf{1}\cdot H_2O$ were performed in the 1.8−15 K range using a 3.5 G ac field oscillating at frequencies in

(34) (a) King, P.; Wernsdorfer, W.; Abboud, K. A.; Christou, G. *Inorg. Chem.* **2004**, *43*, 7315. (b) Manoli, M.; Prescimone, A.; Mishra, A.; Parsons, S.; Christou, G.; Brechin, E. K. *Dalton Trans.* **2007**, 532. (c) Konar, S.; Clearfield., A. *Inorg. Chem.* **2008**, *47*, 3489.

(35) (a) Dey, S. K.; Abedin, T. S. M.; Dawe, L. N.; Tandon, S. S.; Collins, J. L.; Thompson, L. k.; Postnikov, A. V.; Alam, M. S.; Müller, P. *Inorg. Chem.* **2007**, *46*, 7767. (b) Liu, W.; Lee, K.; Park, M.; John, R. P.; Moon, D.; Zou, Y.; Liu, X.; Ri, H.-C.; Kim, G. H.; Lah, M. S. *Inorg. Chem.* **2008**, *47*, 8807. (c) Lee, J.; Gorun, S. M. *Angew. Chem., Int. Ed.* **2003**, *42*, 1512.

(36) Davidson, E. R. *MAGNET*; Indiana University: Bloomington, IN, 1999.

(37) (a) Soler, M.; Wernsdorfer, W.; Folting, K.; Pink, M.; Christou, G. *J. Am. Chem. Soc.* **2004**, *126*, 2156. (b) Brechin, E. K.; Sañudo, E. C.; Wernsdorfer, W.; Boskovic, C.; Yoo, J.; Hendrickson, D. N.; Yamaguchi, A.; Ishimoto, H.; Concolino, T. E.; Rheingold, A. L.; Christou, G. *Inorg. Chem.* **2005**, *44*, 502. (c) King, P.; Wernsdorfer, W.; Abboud, K. A.; Christou., G. *Inorg. Chem.* **2005**, *44*, 8659.

(38) (a) Murugesu, M.; Raftery, J.; Wernsdorfer, W.; Christou, G.; Brechin, E. K. *Inorg. Chem.* **2004**, *43*, 4203. (b) Scott, R. T. W.; Parsons, S.; Murugesu, M.; Wernsdorfer, W.; Christou, G.; Brechin, E. K. *Angew. Chem., Int. Ed.* **2005**, *44*, 6540.

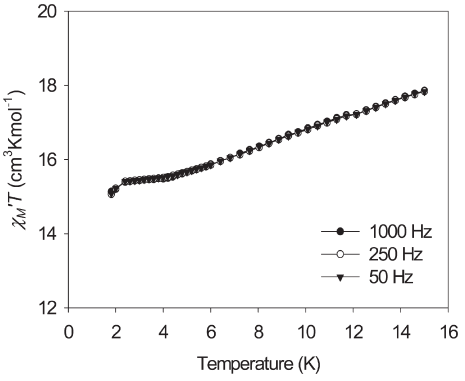

Figure 5. In-phase ac susceptibility of complex **1** in a 3.5 G field oscillating at the indicated frequencies. A small spike at 2.2 K, an artifact of the liquid He triple point, has been removed.

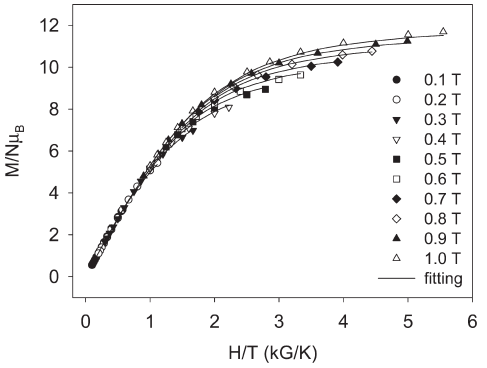

Figure 6. Plots of reduced magnetization ($M/N\mu_B$) versus H/T for complex **2**. The solid lines are the fit of the data; see the text for the fit parameters.

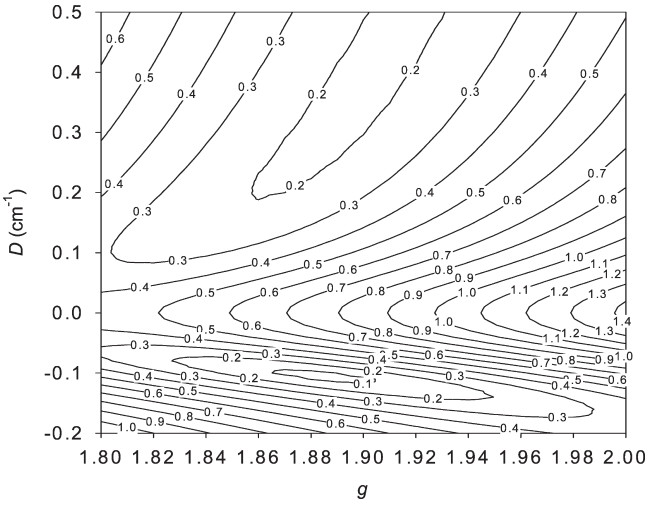

Figure 7. Two-dimensional contour plot of the root-mean-square error surface for the D versus g fit of Figure 6 for complex **2**.

the 50−1000 Hz range. The obtained in-phase ac susceptibility data (χ_M', plotted as $\chi_M'T$) are shown in Figure 5. In the absence of slow magnetization relaxation and a resulting out-of-phase (χ_M'') signal, the ac $\chi_M'T$ is equal to the dc χ_MT, allowing determination of the ground state S in the absence of a dc field. The $\chi_M'T$ values decrease significantly with decreasing temperature, indicating depopulation of one or more excited states with S greater than the ground state S, rationalizing the problematic fits of dc magnetization data. Extrapolation of the plot from above 4 to 0 K (to avoid dips at the lowest temperature due to anisotropy, weak intermolecular interactions, etc.), where only the ground state will be populated, gives a $\chi_M'T$ value of ~15 cm^3 K mol^{-1}, which is the value expected for an $S = 5$ state with $g \sim 2$. An $S = 4$ or $S = 6$ ground state would give a $\chi_M'T$ value of ~10 or ~21 cm^3 K mol^{-1}, respectively, clearly very different from the experimental data. We thus feel confident in our conclusion that **1** has an $S = 5$ ground state. Complex **1** exhibited no out-of-phase (χ_M'') ac signal down to 1.8 K, indicating that it does not exhibit a significant barrier (versus kT) to magnetization relaxation, that is, it is not an SMM.

Magnetic Susceptibility Study of Complex 2. Variable-temperature dc magnetic susceptibility data for complex **2**·H_2O were collected as for **1**·H_2O, and are shown as a χ_MT versus T plot in Figure 4. χ_MT gradually decreases from 42.52 cm^3 K mol^{-1} at 300 K to a minimum of 30.33 cm^3 K mol^{-1} at 15.0 K, and then slightly increases to 31.17 cm^3 K mol^{-1} at 5 K. The 300 K value is less than the spin-only ($g = 2$) value of 56.25 cm^3 K mol^{-1} for six Mn^{II} and ten Mn^{III} non-interacting ions, indicating the presence of antiferromagnetic interactions, but the χ_MT versus T profile suggests there may also be significant ferromagnetic interactions as well. The 5.0 K value is indicative of an $S = 8$ ground state ($\chi_MT = 36.00$ cm^3 K mol^{-1} for $g = 2$).

Magnetization data for **2**·H_2O were collected at different fields and temperatures, as for **1**·H_2O, and attempts were made to fit them by matrix diagonalization, but again we could not obtain a satisfactory fit using all data up to 7 T. This time, however, we were able to get an acceptable fit using only data collected at low fields, consistent with the stronger exchange interactions expected for the higher oxidation level and greater OH^-/O^{2-} content of **2** versus **1**, and a resulting bigger separation to excited states. The data are shown as a reduced magnetization ($M/N\mu_B$) versus H/T plot in Figure 6, where N is Avogadro's number, and the fit (solid lines in Figure 6) gave $S = 8$, $D = -0.11$ cm^{-1}, and $g = 1.89$. Alternative fits with $S = 7$ or 9 were rejected because they gave unreasonable values of g. The root-mean-square D versus g error surface for the fit was generated using the program GRID,[39] and is shown as a 2-D contour plot in Figure 7 for the $D = -0.2$ to 0.5 cm^{-1} and $g = 1.8$ to 2.0 ranges. Two fitting minima are observed with positive and negative D values, with the latter being clearly superior and supporting the D for **2**·H_2O being negative. From the shape and orientation of the contour describing the region of minimum error, we estimate the precision/uncertainty of the fit parameters as $S = 8$, $D = -0.11(1)$ cm^{-1} and $g = 1.89(3)$.

The in-phase (χ'_MT) and out-of-phase (χ''_M) ac susceptibilities for **2** are shown in Figure 8. $\chi_M'T$ steadily increases with decreasing temperature from a value of ~32 cm^3 K mol^{-1} at 15 K to a value of ~34 cm^3 K mol^{-1} at 2.2 K before exhibiting a small decrease. The $\chi_M'T$ values at the lowest temperatures clearly indicate an $S = 8$ ground state with $g \sim 2.0$, in agreement with the dc magnetization fit. $S = 7$ and 9 ground states would give

(39) Davidson, E. R. *GRID*; Indiana University: Bloomington, IN, 1999.

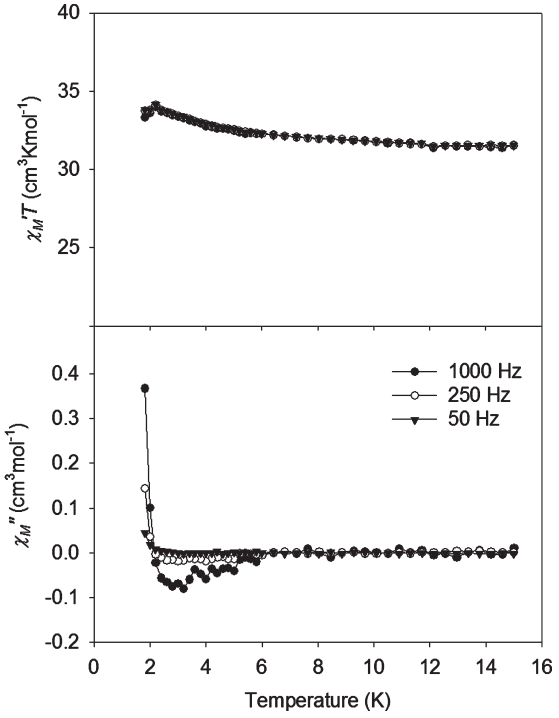

Figure 8. AC susceptibility of complex **2** in a 3.5 G field oscillating at the indicated frequencies: (top) in-phase signal (χ_M') plotted as $\chi_M'T$ versus T; and (bottom) out-of-phase signal χ_M'' versus T. The small spike at 2.2 K is an artifact of the liquid He triple point.

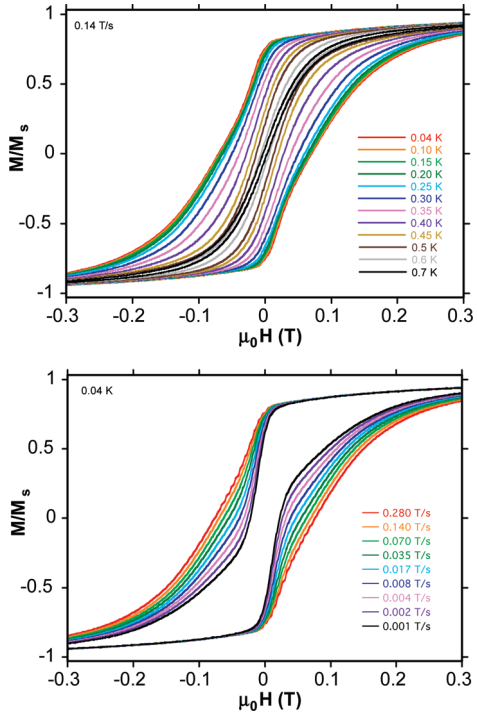

Figure 9. Magnetization (M) versus dc field hysteresis loops for a single crystal of **2**·10MeOH at (top) the indicated temperatures and field sweep rate; and (bottom) the indicated field sweep rates and temperature. The magnetization is normalized to its saturation value, M_S.

$\chi_M'T$ values of ~28.0 and ~45.0 cm^3 K mol^{-1}, respectively, clearly very different from the experimental value. We thus conclude that complex **2**·H_2O has an $S = 8$ ground state. Frequency-dependent out-of-phase χ_M'' signals, which are clearly the tails of peaks whose maxima are at < 1.8 K, were observed at temperatures below 3 K, indicating slow magnetization relaxation and suggesting that **2**·H_2O might be a SMM. If so, it should exhibit magnetization hysteresis, and this was therefore explored.

Hysteresis Studies below 1.8 K. Magnetization versus applied dc field studies were performed on single crystals of **2**·10MeOH (maintained in contact with mother liquor) at temperatures down to 0.04 K using a micro-SQUID apparatus.[25] Hysteresis loops were observed below 0.7 K, whose coercivities increase with decreasing temperature and increasing field sweep rate (Figure 9), as expected for the superparamagnetic-like properties of a SMM below its blocking temperature (T_B). The data thus confirm complex **2**·10MeOH to be a new addition to the family of SMMs, but do not show the steps characteristic of quantum tunneling of magnetization (QTM). This is as expected for high nuclearity SMMs since they are more susceptible to various step-broadening effects from low lying excited states, intermolecular interactions, and/or distributions of local environments owing to ligand and solvent disorder.

To estimate the effective kinetic barrier U_{eff} to relaxation, the magnetization was first saturated in one direction at ~5 K with a large dc field, the temperature decreased to a chosen value, the field removed, and the magnetization decay monitored with time. The results are shown in Supporting Information, Figure S2. This provided magnetization relaxation time (τ) versus

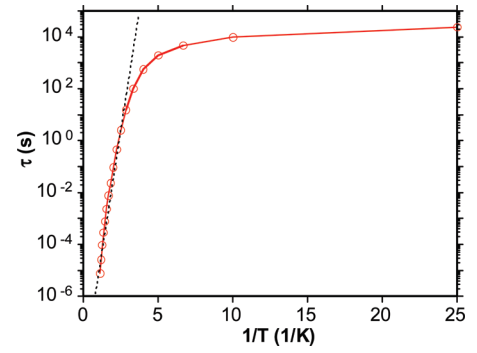

Figure 10. Arrhenius plot of the relaxation time (τ) versus $1/T$ for a single crystal of **2**·10MeOH. The dashed line is the fit of the data in the thermally activated region to the Arrhenius equation; see the text for the fit parameters.

temperature data, shown as a τ versus $1/T$ plot in Figure 10 based on the Arrhenius relationship of eq 4, where τ_0 is

$$\tau = \tau_0 \exp(U_{eff}/kT) \quad (4)$$

the pre-exponential factor, U_{eff} is the mean effective barrier, and k is the Boltzmann constant. The fit of the thermally activated region, shown as the dashed line in Figure 10, gave $U_{eff} = 8.1$ K and $\tau_0 = 4 \times 10^{-9}$ s. The U_{eff} is, as expected, smaller than the upper limit of the barrier, U, given by $S^2|D|$ for integer S; for the $S = 8$ and $D = -0.11$ cm^{-1} values obtained for **2**·H_2O from the magnetization fits, $U = 7.0$ cm^{-1} = 10.1 K. Thus, $U_{eff} < U$, consistent with QTM through upper regions of the barrier decreasing the effective barrier height. The presence of QTM in **2** is also evident in Figure 10 where the relaxation time at the lowest temperatures becomes essentially

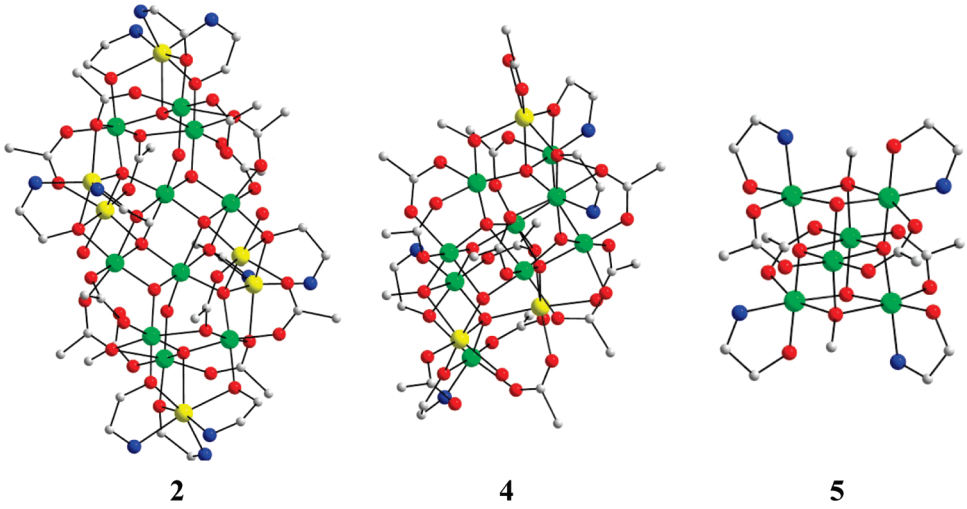

Figure 11. Comparison of the cores of **2**, **4**, and **5**. For clarity, only the C atoms connecting the O and N atoms of the chelates are shown. Color code: Mn^{II}, yellow; Mn^{III}, green; O, red; C, gray; N, blue.

temperature−independent, characteristic of relaxation only via the lowest energy $M_S = \pm 8$ levels of the $S = 8$ spin manifold.

Comparison of hmp$^-$ (2), dmhmp$^-$ (4), and dphmp$^-$ (5) Mn Clusters. As stated in the Introduction, we sought and now have a triad of Mn_x clusters prepared under exactly the same conditions but differing in the chelate employed. It was important to do so, because factors such as reagent ratio, the carboxylate employed, reaction solvent, and so forth are particularly influential in Mn cluster chemistry, and we wanted to ensure as much as possible that the identity of the product would reflect the bulk, electronic properties, and binding preferences of the chelate. The cores of the three compounds $[Mn_{16}O_8(OH)_2(O_2CPh)_{12}(hmp)_{10}(H_2O)_2]^{2+}$ (cation of **2**), $[Mn_{12}O_7(OH)(OMe)_2(O_2CPh)_{12}(dmhmp)_4(H_2O)]$ (**4**), and $[Mn_6O_4(OMe)_2(O_2CPh)_4(dphmp)_4]$ (**5**) are shown in Figure 11. The following observations can be made:

(i) The compounds show a decreasing Mn_x nuclearity with increasing chelate bulk.

(ii) The O atoms of hmp$^-$ adopt both μ_3- and μ_2-bridging modes, those of bulkier dmhmp$^-$ are all μ_2, and those of dphmp are all μ_1, that is, terminal.

(iii) The two relatively small Me groups in dmhmp$^-$ can be considered merely a perturbation of hmp$^-$. Thus, although the nuclearity has decreased from **2** (Mn_{16}) to **4** (Mn_{12}) and the Mn/chelate ratio increases from 16:10 (**2**) to 12:4 (**4**), the two compounds still show some structural similarities. In particular, they both contain a $[Mn_4(\mu_4\text{-}O^{2-})]$ tetrahedron either side of a central unit: for **2**, this is a linked Mn_8 dicubane, whereas for **4** it is a smaller $[Mn_4(\mu\text{-}O^{2-})_6]$ face-fused incomplete dicubane (two face-sharing cubanes each missing a Mn atom). This point is consistent with the presence of μ_3 modes for the hmp$^-$ O atoms in the Mn_8 dicubane, which has never been seen for dmhmp$^-$ (vide infra).

(iv) The much bulkier dphmp$^-$ does not bridge but instead binds as a chelate and gives a very different type of product, although it does also contain a complete dicubane, albeit face-fused rather than just linked as in **2**.

The above conclusions support the increasing bulk of the substituents next to the O atom of the chelate, and the resulting differing O binding preferences, as the primary cause of the differing products. This is supported by the list in Table 7 of known Mn complexes with these chelates, and a clear trend can be seen to lower μ_n-bridging modes as the bulk of the chelate increases. The dphmp$^-$ has never displayed a μ_2 mode, only the occasional semibridging ($n = 1.5$) situation where a weak, long (> 2.4 Å) contact to a second metal is formed.

Table 7. Complexes with hmp$^-$, dmhmp$^-$, or dphmp$^-$, and their Alkoxide Binding Mode

complex[a]	n (μ_n-O)[b,c]	ref
$[Mn_4O_2(O_2CPh)_7(hmp)_2]^-$	1	17
$[Mn_4(hmp)_6X_{4-x}(solv)_x]^{z+}$ [d]	3	20, 21
$[Mn_4(6\text{-Me-hmp})_6Cl_4]$	3	20a
$[Mn_4(hmp)_4Br_2(OMe)_2(dcn)_2]$	3	20c
$[Mn_4(hmp)_4(acac)_2(MeO)_2]^{2+}$	2	21d
$[Mn_7(OH)_3(hmp)_9Cl_3]^{2+}$	2, 3	18a
$[Mn_8O_2(O_2CPh)_{10}(hmp)_4(MeOH)_2]$ (**1**)	3	t.w.
$[Mn_{10}O_4(OH)_2(O_2CMe)_8(hmp)_8]^{4+}$	2, 3	18a
$[Mn_{10}O_4(N_3)_4(hmp)_{12}]^{2+}$	2	18c
$[Mn_{12}O_8Cl_4(O_2CPh)_8(hmp)_6]$	2	18b
$[Mn_{16}O_8(OH)_2(O_2CPh)_{12}(hmp)_{10}(H_2O)]^{2+}$ (**2**)	2, 3	t.w.
$[Mn_{21}O_{14}(OH)_2(O_2CMe)_{16}(hmp)_8(pic)_2(py)(H_2O)]^{4+}$	2	19
$[Mn_7O_3(OH)_3(O_2CBu^t)_7(dmhmp)_4]$	1, 2	22b
$[Mn_{12}O_7(OH)(OMe)_2(O_2CPh)_{12}(dmhmp)_4(H_2O)]$ (**4**)	2	22b
$[Mn_4O_2(O_2CBu^t)_5(dphmp)_3]$	1, 1.5[c]	22a
$[Mn_6O_4(OMe)_2(O_2CPh)_4(dphmp)_4]$ (**5**)	1	22a
$[Mn_{11}O_7(OMe)_7(O_2CPh)_7(dphmp)_4(MeOH)_2]$	1, 1.5[c]	22a

[a] Counterions omitted. [b] Bridging mode of the hmp$^-$, dmhmp$^-$, or dphmp$^-$ O atom; μ_1-O indicates a non-bridging (terminal) mode. [c] $n = 1.5$ refers to a semi-bridging mode. [d] Many complexes, varying in the content of monodentate anionic ligand X^- and solvent molecules (solv). t.w. = this work.

Conclusions

We have reported two new Mn_8 (**1**) and Mn_{16} (**2**) clusters with hmp$^-$ and shown that the latter is a new SMM with an $S = 8$ ground state. In addition, **2** joins **4** and **5** to give a family of clusters prepared under the same conditions except for the chelate, and they have different structures that can be rationalized on the basis of the increasing bulk of the

substituents next to the alkoxide O atom and their influence on the resulting binding mode. Since the alkoxide O atoms of the hmp^- groups each bridging two or three Mn atoms is a main reason that a high nuclearity complex is formed, it makes sense that bulkier chelates with lower μ_n should give lower nuclearity products; in addition, the number of chelates that can be fit around a cluster is obviously affected. However, this is not to say that, for example, $dphmp^-$ cannot give high nuclearity clusters because it cannot bridge—as can be seen in Table 7, a Mn_{11} cluster is known with this chelate, its many μ_2 and μ_3 MeO^- groups replacing the $dphmp^-$ alkoxide O atoms as contributors (with the oxides) to the resulting high nuclearity. Notwithstanding such examples, the overall picture that emerges is that controlled modification of a chelate by addition of substituents of a chosen size is a valuable way to access new M_x clusters with very rare or prototypical metal topologies. Finally, we realize with hindsight that $dmhmp^-$ is fairly similar to hmp^-, and $dphmp^-$ is very different, and as a result it would be of interest to also investigate the use of a chelate with substituents intermediate in bulk between Me and Ph, such as Pr^i, and this is currently under investigation.

Acknowledgment. G.C. thanks the National Science Foundation for support of this work through Grant CHE-0910472. W.W. thanks the financial support from the ANR-PNANO projects MolNanoSpin ANR-08-NANO-002 and the ERC Advanced Grant MolNanoSpin 226558.

Supporting Information Available: X-ray crystallographic data in CIF format for complexes **1**·$2CH_2Cl_2$ and **2**·10MeOH. This material is available free of charge via the Internet at http://pubs.acs.org.